Electromagnetic guiding of vertical transportation vehicles: state control of an over-determined system

Benedikt Schmülling, Rüdiger Appunn, and Kay Hameyer
Institute of Electrical Machines, RWTH Aachen University,
Schinkelstraße 4, D-52056 Aachen, Germany
phone: (+49)-241-80-97667, fax: (+49)-241-80-92270
E-mail: Benedikt.Schmuelling@iem.rwth-aachen.de

Abstract— **This paper describes the design of a state controller for an electromagnetic elevator guiding system. One challenge of this design is the over-determination of the mechanical system due to its high number of adjustment variables. Force decoupling, the transformation of local and global quantities, and simulation results of the entire system are presented in this paper.**

I. Introduction

Conventional elevators consist of an elevator car in a shaft operated by a rope, which is mounted on a traction sheave. The mechanical guiding of such elevators is well-known. Usually, slideways or roller guides are used.

However, conventional guides show several disadvantages when compared to a contactless solution. The higher speed, required for an efficient passenger transportation in high-rise buildings yields a faster deterioration. Conventional guides require lubricants and a regular maintenance. Further benefits of contactless guides are the higher comfort obtained by audible noise reduction and a controllable guiding stiffness.

II. Degrees of freedom

The elevator car is assumed to be a rigid body. It is fixed in one degree of freedom (DOF) by its propulsion device, a rope for example. This is the DOF in vertical z direction. The other five DOF are the translatory movements in x and y direction and the rotary movements α, β, and γ around the axes of a Cartesian coordinate system located at the gravity centre of the elevator car. These five DOF have to be controlled by electromagnetic fields.

III. Guiding topology

A. Actuators

An important component of the guideway is the so called guiding shoe, which transmits disturbance forces from the elevator car to the guide rail. As aforementioned, conventional guiding shoes are constructed using rollers or slideways.

The electromagnetic alternative presented is the three-armed actuator (TAA) [1]. The TAA is an electromagnetic actuator able to excite three independent pulling forces. This is a significant improvement with respect to conventional u-shaped actuators [2], which generate a pulling force in one direction only. Therefore, one TAA replaces three u-actuators. A further actuator is the magnet module presented in [3], which controls one complete DOF, i.e. producing a force in one direction (positive and negative). Nevertheless, the TAA controls one and a half DOF. Therewith, two TAAs substitute three magnet modules.

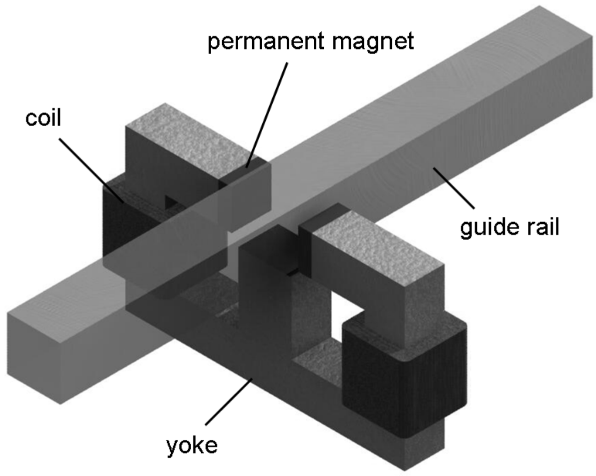

Fig. 1. TAA on a guide rail.

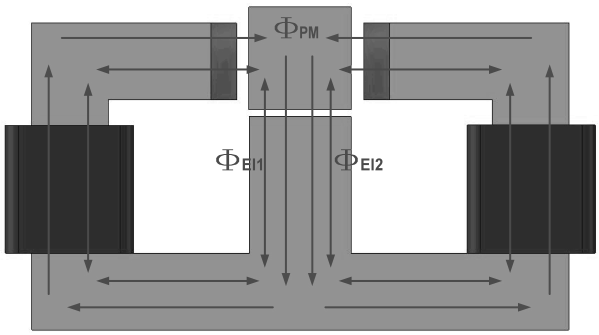

Fig. 2. Superposed fluxes in a TAA's cross-section.

Fig. 1 shows the schematic of a TAA. It consists of a three-armed iron yoke, mounted with permanent magnets on the outer pole surfaces, and coils around the lateral arms.

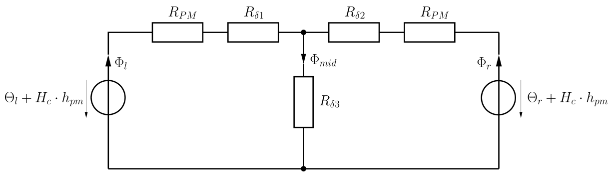

Fig. 3. Magnetic equivalent circuit of the TAA.

The operation of this actuator is based on the superposition of a permanent magnet flux Φ_{PM} with electrically excited fluxes Φ_{El1} and Φ_{El2}. The cross-section and the fluxes in the actuator are presented in Fig. 2. The analytical calculation of the actuator's magnetic fluxes is based on the method of the magnetic equivalent circuit (MEC), which works analogue to an electrical equivalent network. At first, sources and magnetic resistances (reluctances) are determined. As a first approximation the reluctance of the iron yokes and the guide rail is neglected due to their high permeability compared to that of the air gaps. The reluctances of air gap R_δ and permanent magnet R_{PM} are determined as follows:

$$R_\delta = \frac{\delta}{\mu_0 A} \tag{1}$$

and

$$R_{PM} = \frac{h_{pm} H_c}{B_r A}, \tag{2}$$

where A is the cross-section of the air gap, μ_0 is the permeability of the vacuum, H_c is the coercivity and B_r is the remanence of the permanent magnet. δ and h_{pm} are the permeated heights of air gap and magnet respectively. The magnetic voltage sources in the MEC are the two permanent magnets and the two coils. The magnetomotive force (MMF) of one coil is defined as $\Theta = w \cdot i$ and the MMF of one magnet equals to $H_c \cdot h_{pm}$. With this information the resulting equivalent network of the magnetic circuit can be established (Fig. 3).

During operation, the three guiding forces occur in the air gaps of the actuator/guide rail system. They depend on the air gap fluxes Φ_r, Φ_l, and Φ_y. From the MEC, it can be seen that each force depends on all air gaps and all MMFs. Thus, a mathematical decoupling of the forces is required to design an adequate control system.

B. Complete system

The actuators are mounted on opposite edges of roof and floor of the elevator car, i. e. four TAAs are mounted on one car. In combination with two guide rails located on opposite walls of the elevator shaft, the complete guiding system is formed (Fig. 4). Altogether, the four TAAs produce twelve pulling forces, organised in pairs along six action lines. Hence, a total of six forces remain to control the position of the elevator car, i. e. to control the five degrees of freedom (x, y, α, β, and γ). These forces are depicted in Fig. 5. On the left hand side, the twelve individual forces are presented. On the right hand side the forces acting on the same line are merged into

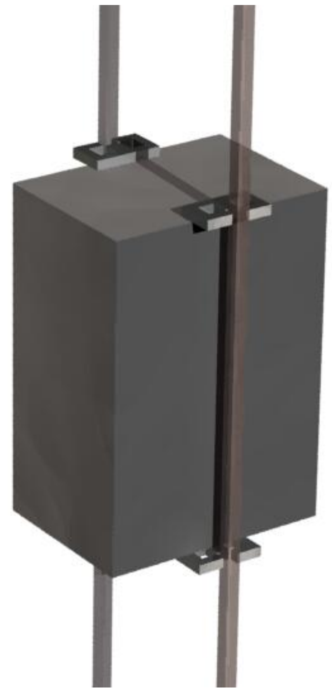

Fig. 4. Elevator car guided by four TAAs.

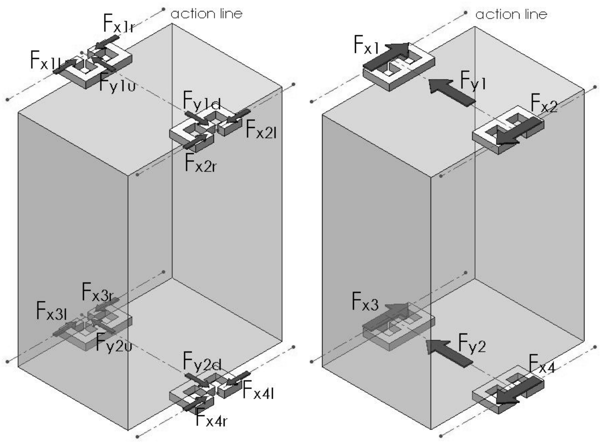

Fig. 5. Individual forces (left) and superposed forces (right) of all TAAs.

the six control forces F_{x1}, F_{x2}, F_{x3}, F_{x4}, F_{y1}, and F_{y2}. Due to the fact that the three forces of each TAA are driven by two coils, eight linearly independent current variables are available for adjusting them. Therefore, the guiding of an elevator car by means of TAAs necessitates a feedback control of an over-determined system.

C. Linearisation

The implementation of a state space controller requires a linear time-invariant (lti) system. The pulling force F between an actuator arm and the guide rail can be approximated by

$$F = \frac{\Phi^2}{2\mu_0 A}, \tag{3}$$

with the magnetic flux Φ calculated with the MEC described above. The dependence of F on the magnetic flux Φ is quadratic. Thus, the guiding system is non-linear. The flux is given by

$$\Phi = f(\Theta_l, \Theta_r, \delta_x, \delta_y), \tag{4}$$

with $f(...)$ as a complicated function.

Let us define the air gap vector

$$\boldsymbol{\delta} = (\delta_{x1}\ \delta_{y1}\ \delta_{x2}\ \delta_{y2}\ \delta_{x3}\ \delta_{y3}\ \delta_{x4}\ \delta_{y4}\ )^T \tag{5}$$

and

$$\boldsymbol{\Theta} = (\Theta_{r1}\ \Theta_{l1}\ \Theta_{r2}\ \Theta_{l2}\ \Theta_{r3}\ \Theta_{l3}\ \Theta_{r4}\ \Theta_{l4}\ )^T \tag{6}$$

as two eight component vectors containing the TAA variables. For the purpose of designing the controller, the expressions of TAA fluxes and forces in terms of those variables need to be linearised around a working point (WP). One defines

$$\boldsymbol{\delta} = \boldsymbol{\delta_0} + \boldsymbol{\Delta\delta} \tag{7}$$

$$\boldsymbol{\Theta} = \boldsymbol{\Theta_0} + \boldsymbol{\Delta\Theta} \tag{8}$$

with all components of $\boldsymbol{\Theta}$ equal to zero and all components of $\boldsymbol{\delta}$ equal to $3\,\mathrm{mm}$, which correspond to the car being centred in the shaft. One has for each TAA the linearised fluxes:

$$\begin{aligned}
&\Phi_{ik}(\Delta\delta_{xk}, \Delta\delta_{yk}, \Delta\Theta_{lk}, \Delta\Theta_{rk}) = \Phi_{ij0}\\
&+ \left[\frac{\partial\Phi}{\partial\Delta\delta_{xk}}\right]_{\Theta_{0rk},\Theta_{0lk},\delta_{0xk},\delta_{0yk}} \Delta\delta_{xk}\\
&+ \left[\frac{\partial\Phi}{\partial\Delta\delta_{yk}}\right]_{\Theta_{0rk},\Theta_{0lk},\delta_{0xk},\delta_{0yk}} \Delta\delta_{yk}\\
&+ \left[\frac{\partial\Phi}{\partial\Delta\Theta_{lk}}\right]_{\Theta_{0rk},\Theta_{0lk},\delta_{0xk},\delta_{0yk}} \Delta\Theta_{lk}\\
&+ \left[\frac{\partial\Phi}{\partial\Delta\Theta_{rk}}\right]_{\Theta_{0rk},\Theta_{0lk},\delta_{0xk},\delta_{0yk}} \Delta\Theta_{rk},
\end{aligned} \tag{9}$$

$$with\ j = l \vee r,\ i = x \vee y, and\ k = 1, ..., 4.$$

The control voltage of one coil, which depends on the MMF and the air gap heights, writes

$$\begin{aligned}
U_{jk}(\Delta\Theta_{jk}, \Phi_j k) = &\frac{R}{N}\Theta_{jk}\\
&+ w\frac{d}{dt}\Phi_{jk}(\Delta\delta_{xk}, \Delta\delta_{yk}, \Delta\Theta_{lk}, \Delta\Theta_{rk}),
\end{aligned} \tag{10}$$

with w as the number of winding turns. Merging (9) and (10) and solving the equation for the MMF yields the differential current equation.

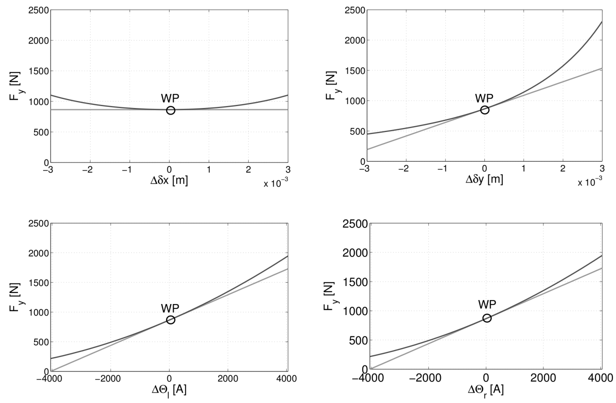

Fig. 6. Comparison between linearised and original forces.

The linearised force results to

$$\begin{aligned}
&F_{ik}(\Delta\delta_{xk}, \Delta\delta_{yk}, \Delta\Theta_{lk}, \Delta\Theta_{rk}) = F_{i0}\\
&+ \left[\frac{\partial F}{\partial\Delta\Theta_{lk}}\right]_{\Theta_{0rk},\Theta_{0lk},\delta_{0xk},\delta_{0yk}} \Delta\Theta_{lk}\\
&+ \left[\frac{\partial F}{\partial\Delta\Theta_{rk}}\right]_{\Theta_{0rk},\Theta_{0lk},\delta_{0xk},\delta_{0yk}} \Delta\Theta_{rk}\\
&+ \left[\frac{\partial F}{\partial\Delta\delta_{xk}}\right]_{\Theta_{0rk},\Theta_{0lk},\delta_{0xk},\delta_{0yk}} \Delta\delta_{xk}\\
&+ \left[\frac{\partial F}{\partial\Delta\delta_{yk}}\right]_{\Theta_{0rk},\Theta_{0lk},\delta_{0xk},\delta_{0yk}} \Delta\delta_{yk}.
\end{aligned} \tag{11}$$

Fig. 6 shows the difference between the original and the linearised force values (for F_y) in dependence to every influence quantity.

IV. The State Space Model

Elevator cars for passenger transportation have a typical rated load of 630 Kg. It is supposed to behave like a rigid body. The dynamic model consists of the mechanical equations of the elevator car and the electromagnetic equations of the four actuators. One defines the position vector of the car:

$$\mathbf{q} = (x\ y\ \alpha\ \beta\ \gamma)^T. \tag{12}$$

The force of the actuators depends on the air gap heights, which have to be calculated from the vehicle position. Reciprocally, the forces of the actuators have to be converted into the elevator car coordinates. Therefore, a mapping between $\mathbf{q}$ and the TAA variables is established.

A. Transformation of local quantities

The components of $\mathbf{q}$ are global quantities. However, the measured quantities on the elevator car are the local air gaps. Thus, a transformation has to be performed to control $\mathbf{q}$ with the aid of the sensor signals. In Fig. 7, the positioning of six air gap sensors is presented. It can be seen, that six air gaps are observed, although there are only five DOF. Here, for the transformation to the global quantities, only five air

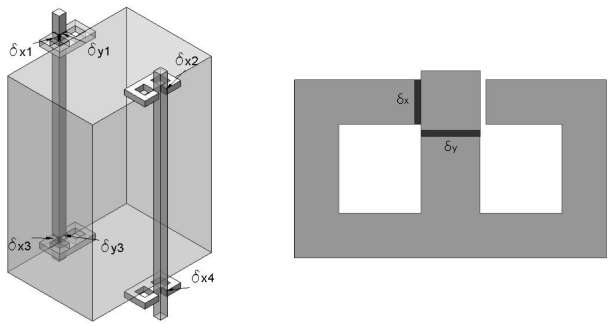

Fig. 7. Observed air gaps.

gap sensor signals are required in principle. However, due to manufacturing tolerances the calculation of the spatial position is easier with additional sensors. The vector of the observed air gaps is

$$\boldsymbol{\delta_{sensor}} = (\delta_{x1}\ \delta_{y1}\ \delta_{x2}\ \delta_{x3}\ \delta_{y3}\ \delta_{x4})^T. \tag{13}$$

For instance, the translatory movement in x direction is deduced from the arithmetic average of four air gap heights:

$$x = \frac{1}{4}(\Delta\delta_{x1} - \Delta\delta_{x2} + \Delta\delta_{x3} - \Delta\delta_{x4}). \tag{14}$$

The signs of opposite actuators are different. The translatory movement in y direction is calculated similarly, but only two air gaps are available:

$$y = \frac{1}{2}(\Delta\delta_{y1} + \Delta\delta_{y3}). \tag{15}$$

The angular positions are deduced from the local quantities by means of trigonometrical relationships. For α follows

$$\alpha = \arctan(\frac{-\Delta\delta_{y1} + \Delta\delta_{y3}}{h}), \tag{16}$$

where h is the vertical distance between two TAAs. By use of the small-angle approximation follows

$$\alpha = \frac{-\Delta\delta_{y1} + \Delta\delta_{y3}}{h}. \tag{17}$$

This approximation is valid, since the maximum value of the tilt angle is $\alpha = 0.17\,^\circ$, when the TAA hits upon the guide rail. The determination of β and γ occurs similarly. Finally, the transformation to global quantities writes

$$\mathbf{q} = \mathbf{T} \cdot \boldsymbol{\delta_{sensor}}, \tag{18}$$

where $\mathbf{T}$ is the transformation matrix

$$\mathbf{T} = \begin{bmatrix} 1/4 & 0 & -1/4 & 1/4 & 0 & -1/4 \\ 0 & 1/2 & 0 & 0 & 1/2 & 0 \\ 0 & -1/h & 0 & 0 & 1/h & 0 \\ 1/2h & 0 & -1/2h & -1/2h & 0 & 1/2h \\ -1/2b & 0 & -1/2b & -1/2b & 0 & -1/2b \end{bmatrix}, \tag{19}$$

with b as the horizontal distance between two TAAs.

B. Force transformation

As aforementioned, the elevator car is assumed to behave like a rigid body. $\mathbf{M}$ is the symmetrical mass matrix, which contains the mass m and the moments of inertia I_x, I_y, I_z of the elevator car:

$$\mathbf{M} = \begin{pmatrix} m & 0 & 0 & 0 & 0 \\ 0 & m & 0 & 0 & 0 \\ 0 & 0 & I_x & 0 & 0 \\ 0 & 0 & 0 & I_y & 0 \\ 0 & 0 & 0 & 0 & I_z \end{pmatrix}. \tag{20}$$

Due to the small angular velocities and due to the fact that there is no physical contact between guide rail and elevator car, the bearing's damping and the Coriolis forces are neglected. The equation system reduces to

$$\mathbf{M}\ddot{\mathbf{q}}(t) = \mathbf{f_{ext}}(\mathbf{t}), \tag{21}$$

with the vector of external forces $\mathbf{f_{ext}}(\mathbf{t})$ acting on the elevator car.

To interact with the equation of motion, the local forces of the TAAs have also be transformed to the vector of the global forces

$$\mathbf{F} = \mathbf{T_F} \cdot \mathbf{f_{local}}, \tag{22}$$

where $\mathbf{f_{local}}$ is the vector of the six control forces, presented in Fig. 5. $\mathbf{T_F}$ is the force transformation matrix:

$$\mathbf{T_F} = \begin{bmatrix} 1 & 0 & -1 & 1 & 0 & -1 \\ 0 & 1 & 0 & 0 & 1 & 0 \\ 0 & -h/2 & 0 & 0 & h/2 & 0 \\ h/2 & 0 & -h/2 & -h/2 & 0 & h/2 \\ -b/2 & 0 & -b/2 & -b/2 & 0 & -b/2 \end{bmatrix}. \tag{23}$$

C. MMF transformation

The eight local MMFs (6) have to be converted to control the five DOF x, y, α, β, and γ. Therefore, the vector of global magnetomotive forces

$$\tilde{\boldsymbol{\Theta}} = (\tilde{\Theta}_x\ \tilde{\Theta}_y\ \tilde{\Theta}_\alpha\ \tilde{\Theta}_\beta\ \tilde{\Theta}_\gamma)^T \tag{24}$$

is introduced. These global MMFs are no physical quantities but decoupled control variables for the adjustment of the global forces $\tilde{F}_x$, $\tilde{F}_y$ and of the global torques $\tilde{M}_\alpha$, $\tilde{M}_\beta$, $\tilde{M}_\gamma$. A symbolic description of the functionality of the global MMFs is displayed in Fig. 8. With the $\mathbf{5 \times 8}$ transformation matrix $\mathbf{T_\Theta}$ the local variables are converted to the global variables:

$$\tilde{\boldsymbol{\Theta}} = \mathbf{T_\Theta} \cdot \boldsymbol{\Theta}, \tag{25}$$

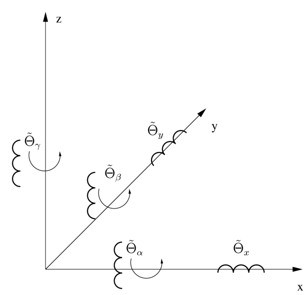

Fig. 8. Global magnetomotive forces.

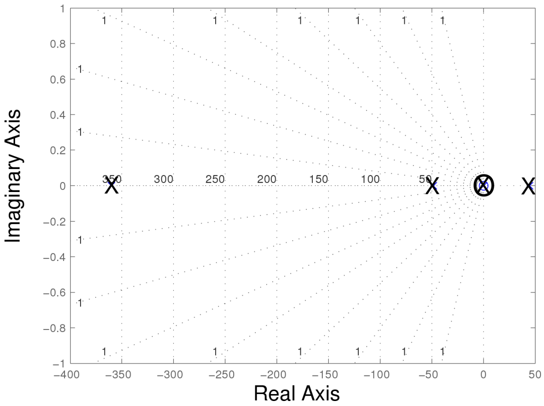

Fig. 9. Pole-zero plot of the uncontrolled DOF x.

with

$$\mathbf{T}_{\boldsymbol{\Theta}} = \frac{\mathbf{1}}{\mathbf{8}} \begin{bmatrix} 1 & -1 & -1 & 1 & 1 & -1 & -1 & 1 \\ 1 & 1 & -1 & -1 & 1 & 1 & -1 & -1 \\ -1 & -1 & 1 & 1 & 1 & 1 & -1 & -1 \\ 1 & -1 & -1 & 1 & -1 & 1 & 1 & -1 \\ -1 & 1 & -1 & 1 & -1 & 1 & -1 & 1 \end{bmatrix}. \tag{26}$$

Each global MMF controls the DOF indicated respectively. With this, the coupling of the forces with all local MMFs is abolished.

One problem of this procedure is the loss of information during the transformation, since the number of adjustment possibilities to achieve one global state with eight local variables is infinite. Thus, an inverse transformation is impossible, but essential for controlling the real magnetomotive forces. Therefore, three global variables with auxiliary information are introduced: $\tilde{\Theta}_{h1}$, $\tilde{\Theta}_{h2}$, and $\tilde{\Theta}_{h3}$. In this variables additional state information is stored during transformation and recalled during the inverse transformation. For the augmented vector of the global MMF results

$$\tilde{\boldsymbol{\Theta}} = (\tilde{\Theta}_x \; \tilde{\Theta}_y \; \tilde{\Theta}_\alpha \; \tilde{\Theta}_\beta \; \tilde{\Theta}_\gamma \; \tilde{\Theta}_{h1} \; \tilde{\Theta}_{h2} \; \tilde{\Theta}_{h3})^T. \tag{27}$$

This augmented MMF vector is calculated by

$$\tilde{\boldsymbol{\Theta}} = \mathbf{T}_{\boldsymbol{\Theta}\mathbf{fnl}} \cdot \boldsymbol{\Theta}. \tag{28}$$

Therefore, the final transformation matrix $\mathbf{T}_{\boldsymbol{\Theta}\mathbf{fnl}}$ for implementing the feedback control is formed:

$$\mathbf{T}_{\boldsymbol{\Theta}\mathbf{fnl}} = \frac{1}{8} \begin{bmatrix} 1 & -1 & -1 & 1 & 1 & -1 & -1 & 1 \\ 1 & 1 & -1 & -1 & 1 & 1 & -1 & -1 \\ -1 & -1 & 1 & 1 & 1 & 1 & -1 & -1 \\ 1 & -1 & -1 & 1 & -1 & 1 & 1 & -1 \\ -1 & 1 & -1 & 1 & -1 & 1 & -1 & 1 \\ 1 & 1 & 1 & 1 & 1 & 1 & 1 & 1 \\ 1 & 1 & 1 & 1 & -1 & -1 & -1 & -1 \\ 1 & -1 & 1 & -1 & -1 & 1 & -1 & 1 \end{bmatrix}. \tag{29}$$

D. Forming the state space equation

The forming of the state space equation for x, the first component of the position vector $\mathbf{q}$ is presented in this section. For the other components the procedure is performed similarly.

Based on the mathematical modelling the system description in state space is deduced from the differential equations of the physical coherences. State variables are the spatial position x, the velocity $\dot{x}$, and the global MMF $\tilde{\Theta}_x$. Additionally, a state space augmentation is implemented. The integral of the spatial position $\int x dt$ is put into the state vector to avoid a permanent deviation. After transforming the linearised force equations (11) and the differential equation of current rise(10) to global quantities, the state space system is obtained:

$$\begin{pmatrix} x \\ \dot{x} \\ \ddot{x} \\ \dot{\tilde{\Theta}}_x \end{pmatrix} = \underbrace{\begin{bmatrix} 0 & 1 & 0 & 0 \\ 0 & 0 & 1 & 0 \\ 0 & -\frac{4}{m}F_{\delta x} & 0 & \frac{8}{m}F_{\Theta x} \\ 0 & 0 & \Theta_{x0} & \Theta_{\Theta 0} \end{bmatrix}}_{A_x} \cdot \begin{pmatrix} \int x dt \\ x \\ \dot{x} \\ \tilde{\Theta}_x \end{pmatrix} + \underbrace{\begin{bmatrix} 0 \\ 0 \\ 0 \\ U_0 \end{bmatrix}}_{B_x} \cdot \left(\tilde{U}_x \right). \tag{30}$$

$$\mathbf{y} = \underbrace{\begin{pmatrix} 0 & 1 & 0 & 0 \end{pmatrix}}_{C_x} \cdot \begin{pmatrix} \int x dt \\ x \\ \dot{x} \\ \tilde{\Theta}_x \end{pmatrix}. \tag{31}$$

Here, $F_{\delta x}$, $F_{\Theta x}$, Θ_{x0}, $\Theta_{\Theta 0}$, and U_0 are linearisation factors. These two equations are the description of the uncontrolled system. A_x is the system matrix, B_x the input matrix, and C_x the output matrix. The feedthrough matrix D_x is chosen to be zero, since there is no direct feedthrough in a real system. Here, $\mathbf{y}$ is not the DOF y, but the output vector of the state space system. Fig. 9 shows the pole-zero plot of the uncontrolled DOF x, which depicts the eigenvalues of the system. It can be seen, that not all poles are placed in the negative half-plane. Therewith, the system is unstable.

V. STATE CONTROL

The control method employed is the so called DOF-control [4]. A benefit of this method compared to a simple air gap control (i.e. every single air gap height is controlled separately) is a higher system stability, against the background of large manufacturing tolerances in high elevator shafts.

A. Controller design

The entire DOF controller is designed with five parallel single state controllers. As presented in section IV, the system matrix is formed and with this the state space equation of the uncontrolled system is established. To stabilise the system, the poles of system matrix A_x have to be replaced. The eigenvalues are adjusted by a feedback of the state vector and a combination with the vector of the input values $\mathbf{u}$. Therefore, control matrix $\mathbf{K_x}$ is introduced. It contains the control parameters, one for every state variable. The controlled system is described by the following equations:

$$\begin{aligned} \dot{\mathbf{x}} &= \mathbf{A_x} \cdot \mathbf{x} + \mathbf{B_x} \cdot \mathbf{u} \\ \mathbf{u} &= -\mathbf{K_x} \cdot \mathbf{x}. \end{aligned} \tag{32}$$

Substituting the latter in the former results in

$$\mathbf{A_K} = \mathbf{A_x} - \mathbf{B_x} \cdot \mathbf{K_x}, \tag{33}$$

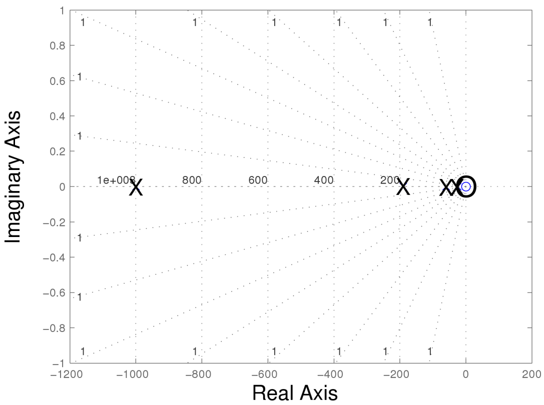

Fig. 10. Pole-zero plot of the controlled DOF x.

with $\mathbf{A_K}$ as the system matrix of the controlled system.

In a further step, the control parameters are computed using the Riccati equation design rules [5]. These rules are based on a minimisation of a squared control quality measure. For the control parameter optimisation, the method of pole placement [5] is used. This method is qualified in several publications. In [6] and [4], the use of this procedure is specified for the application in magnetic levitation controllers. [7] describes the pole placement for a 6-DOF vehicle. Other papers ([8] e.g.) show the implementation of the pole placement for other purposes. Finally, the pole-zero plot of the controlled system is obtained. It is presented in Fig. 10.

The controllers of the other four DOF are designed just as well.

B. Results

The validity of the DOF-control is verified by a dynamic simulation with matlab/simulink. Several real and extreme load cases are computed as well as the stiffness of the guiding system.

Fig. 11 shows the system response to a force impact in x direction, on a defined position upside the barycentre of one wall. It can be seen, that only the DOF x and β are deflected. A couple of force impacts on different positions of the elevator car's walls and floor simulate the real load, i.e. walking and jumping individuals inside. The system response shows a robust guiding characteristic, even in extreme load cases.

The stiffness k of a guiding system is a commonly used comparison criterion. Hereby, quantifiable valuations about bearings and guidings can be performed, which are independent of the load cases. Stiffness k is the reciprocal of the flexibility. It shows a maximum stiffness of $k = 5\,\frac{\mathrm{N}}{\mu\mathrm{m}}$, which is a reasonable value for magnetic levitated systems.

VI. Conclusion

Several real and extreme load cases are computed with the simulation model. The results show a robust state space controller with a high control quality. The topology of this guiding system and its advantages are introduced in the beginning. The functionality of the TAA is explained in detail. Thereafter, it is indicated that the system of four actuators is over-determined. The complete implementation of the 5 DOF state controller is illustrated. Step by step, the force decoupling and the transformation of the local quantities to global variables are demonstrated. Finally results are presented, which show that the system functions correctly.

The implementation of this controller to a real system is projected. An elevator test bench is under construction and the experimental results are going to be presented in a following paper.

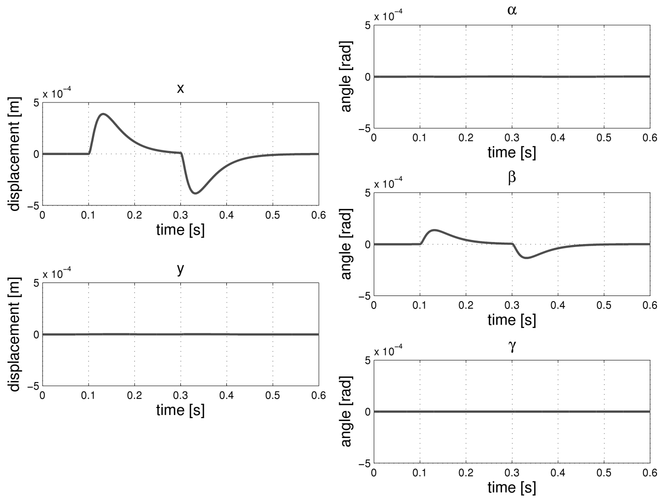

Fig. 11. System response of a force impact in x direction.

References

[1] M. Morishita and M. Akashi, "Electromagnetic non-contact guide system for elevator cars," in *The Third International Symposium on Linear Drives for Industry Applications*. Nagano, Japan: LDIA, October 2001, pp. 416–419.

[2] B. Schmülling, O. Effing, and K. Hameyer, "State control of an electromagnetic guiding system for ropeless elevators," in *European Conference on Power Electronics and Applications*. Aalborg, Denmark: EPE, September 2007, pp. 1–10.

[3] A. Schmidt, C. Brecher, and F. Possel-Dölken, "Novel linear magnetic bearings for feed axes with direct drives," in *International Conference on Smart Machining Systems at the National Institute for Standards and Technology*. Gaithersburg, MD, USA: www.smartmachiningsystems.com, March 2007.

[4] J. Van Goethem and G. Henneberger, "Design and implementation of a levitation-controller for a magnetic levitation conveyor vehicle," in *The 8th International Symposium on Magnetic Bearing*, Mito, Japan, August 2002, pp. 139–142.

[5] O. Föllinger, *Regelungstechnik - Einführung in die Methoden und ihre Anwendung*. Braunschweig: Hüthig Buch Verlag Heidelberg, 1994, 8. Auflage.

[6] Y. S. Lu and J. S. Chen, "Design of a perturbation estimator using the theory of variable-structure systems and its application to magnetic levitation systems," *IEEE Transactions on Industrial Electronics*, vol. 42, no. 3, pp. 281–289, June 1995.

[7] A. S. Ghersin and R. S. Sánchez Peña, "LPV Control of a 6-DOF Vehicle," *IEEE Transactions on Control Systems Technology*, vol. 10, no. 6, pp. 883–887, November 2002.

[8] A. R. Oliva, S. S. Ang, and G. E. Bortolotto, "Digital Control of a Voltage-Mode Synchronous Buck Converter," *IEEE Transactions on Power Electronics*, vol. 21, no. 1, pp. 157–163, January 2006.